Journal of Power Sources 196 (2011) 5000–5006

Contents lists available at ScienceDirect

Journal of Power Sources

journal homepage: www.elsevier.com/locate/jpowsour

Short communication

Ionic conductivity, sintering and thermal expansion behaviors of mixed ion conductor $BaZr_{0.1}Ce_{0.7}Y_{0.1}Yb_{0.1}O_{3-\delta}$ prepared by ethylene diamine tetraacetic acid assisted glycine nitrate process

Xiaoliang Zhou [a,b,c], Limin Liu [c], Jiangman Zhen [c], Shengcai Zhu [c], Baowen Li [c], Kening Sun [b,c,*], Peng Wang [a]

[a] State Key Laboratory of Urban Water Resource and Environment, School of Municipal and Environmental Engineering, Harbin Institute of Technology, Harbin, Heilongjiang 150090, PR China
[b] Natural Science Research Center, Academy of Fundamental and Interdisciplinary Sciences, Harbin Institute of Technology, Harbin, Heilongjiang 150080, PR China
[c] Department of Applied Chemistry, Harbin Institute of Technology, No. 92 of West Dazhi Street, P.O. Box 211, Harbin, Heilongjiang 150001, PR China

ARTICLE INFO

Article history:
Received 25 December 2010
Accepted 23 January 2011
Available online 2 February 2011

Keywords:
Solid oxide fuel cell
Doped barium cerate
Mixed ion conductor
Glycine-nitrate process
AC impedance

ABSTRACT

$BaZr_{0.1}Ce_{0.7}Y_{0.1}Yb_{0.1}O_{3-\delta}$ as a candidate electrolyte material is prepared by ethylene diamine tetraacetic acid assisted glycine-nitrate process. After calcining at 900 °C, the single-phase perovskite is obtained due to the better distribution of starting materials and the more feasible reaction kinetic conditions than solid state reaction method. The relative densities reach 96.8 and 98.4% respectively after sintering the pressed pellets at 1280 and 1400 °C for 10 h. In humidified oxygen the ionic conductivities are 0.015, 0.045, 0.101 and 0.207 S cm^{-1} at 500, 600, 700 and 800 °C, respectively. In air and humidified oxygen the activation energies for ionic conductivity are 66.1 and 68.9 kJ mol^{-1}. In humidified hydrogen, however, different activation energies occur in low and high temperature ranges. The thermal expansion curve inflections at 500–800 °C with respect to possible phase changes are found. Zirconia aggregation possibly results in the higher activation energy and peculiar thermal expansion behavior. The results indicate the ethylene diamine tetraacetic acid assisted glycine-nitrate process is a very promising preparation method for solid oxide fuel cell practical application.

1. Introduction

Due to the high energy conversion efficiency, fuel flexibility including the prospects to operate directly on natural gas and environmental safety, solid oxide fuel cells (SOFCs) are considered as an alternative electric power generation system [1–6]. However, the high operating temperatures (up to 1000 °C) of typical SOFCs with stabilized zirconia as electrolyte lead to complex materials problems including interfacial diffusions, electrode sintering, and the preparation of sealing materials and interconnect. Under these circumstances, intermediate temperature solid oxide fuel cells (IT-SOFCs) are developing very fast because they may avoid these problems [7]. However, reducing operating temperature will significantly increase the ohmic resistance of electrolyte on account of the poor oxygen-ion conductivity of YSZ.

Recently, proton conducting electrolyte materials have attached much attention because they show great advantages over oxide ion conducting ones, such as higher ionic conductivity, lower activation energy and higher energy efficiency [8,9]. Particularly, in proton conducting SOFCs water is formed at the side of cathode. This attracts tremendous attentions in virtue of some advantages over those cells with oxygen ion conducting SOFCs such as simplified fuel-recycling instruments [10,11] and a lower activation energy of proton transport which guarantees that the proton conducting SOFCs operate at an intermediate-to-low temperature range of 400–650 °C. Recently, in order to develop novel electrolyte materials for insufficient conductivity at such low operating temperatures, several proton conducting oxides with attractive ionic conductivities at reduced temperature have been reported [10,12,13].

The state-of-the-art proton conducting materials are barium-based perovskite-type oxides, viz. $BaCeO_3$ and $BaZrO_3$. These materials may obtain adequate proton conductivity as well as sufficient chemical and thermal stability over a wide range of SOFC operating conditions via suitable doping. Yang et al. [14] recently reported BZCYYb ($BaZr_{0.1}Ce_{0.7}Y_{0.1}Yb_{0.1}O_{3-\delta}$) as a novel mixed ion conductor which allowed rapid transport of both protons and oxide ion vacancies and exhibited high ionic conductivity at relatively low temperatures (500–700 °C). Particularly, as compared to other conventional electrolyte materials, e.g. YSZ and GDC, BZCYYb may obtain higher conductivity in lower temperature

* Corresponding author at: Department of Applied Chemistry, Harbin Institute of Technology, No. 92 of West Dazhi Street, P.O. Box 211, Harbin, Heilongjiang 150001, PR China. Tel.: +86 451 86412153; fax: +86 451 86412153.
E-mail address: keningsun@yahoo.com.cn (K. Sun).

0378-7753/$ – see front matter © 2011 Elsevier B.V. All rights reserved.
doi:10.1016/j.jpowsour.2011.01.092

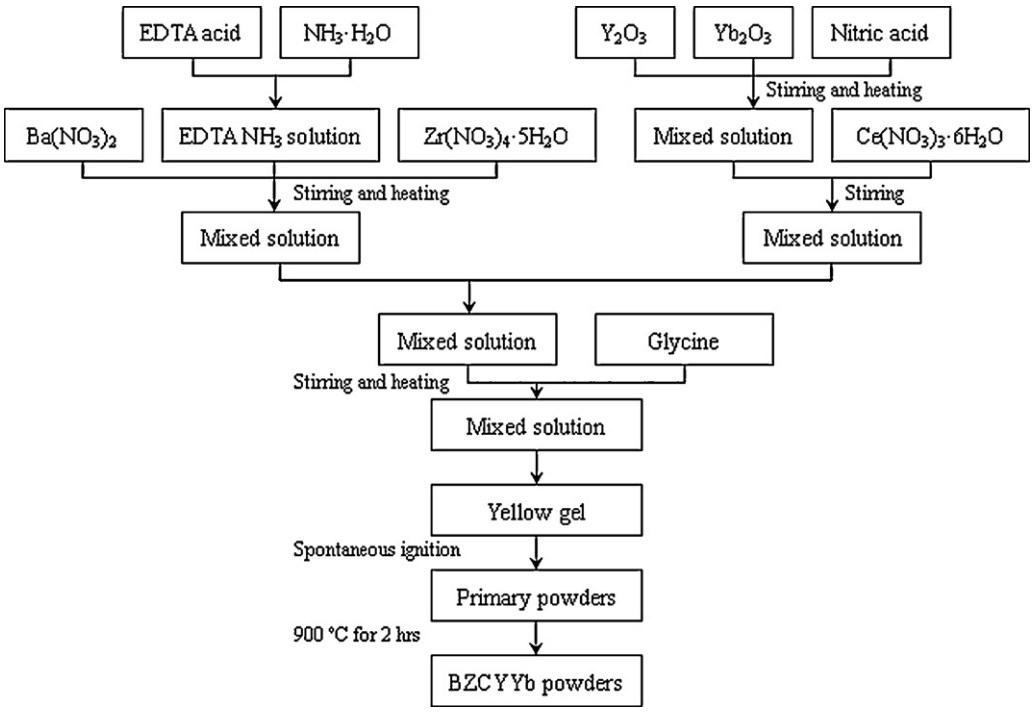

Fig. 1. Flow chart for the preparation of BZCYYb powders by EDTA-assisted GNP method.

ranges. At temperatures below 750 °C, BZCYYb showed the highest ionic conductivity, for example, at 500 °C, the ionic conductivity of BZCYYb was about 1.3×10^{-2} S cm^{-1}, that of $BaZr_{0.1}Ce_{0.7}Y_{0.2}O_{3-\delta}$ (BZCY) was 7×10^{-3} S cm^{-1}, and the ionic conductivity of GDC was 5×10^{-3} S cm^{-1}. On the other hand, this material was also attractive due to its capability to resist deactivation by sulfur and coking with regard to the mixed conductor's enhanced catalytic activity for sulfur oxidation and hydrocarbon cracking and reforming, as well as the enhanced water adsorption ability as a potential anode material.

The materials for SOFCs were generally prepared by mechanical mixing; however the physical mixing cannot ensure the uniform distribution of the material composites leading to poor sintering performance. Combustion process with different fuels was regarded as a very promising one in terms of the physical and chemical homogeneity as well as high crystallinity of obtained powders [15–19]. As a combustion method [20–22], glycine nitrate process (GNP) uses metal nitrates as oxidizers and glycine as fuel to produce ultrafine ceramic powders during a transitory combustion process. The very fine particle size and crystalline nature of the powder produced by GNP are believed to be a direct result of the short exposure to high-temperature during combustion. GNP is also a relatively inexpensive method. It has been adopted for the preparation of simple oxides as well as homogeneous multicomponent oxides [23]. The objective of the present work is to prepare the novel ultrafine electrolyte ceramic powders BZCYYb with high sintering ability by a recently developed EDTA-assisted GNP method and investigate its phase evolution behavior, microstructure of the as-synthesized powders, electrical behavior and thermal expansion characteristics under the cell operating conditions.

2. Experimental

2.1. Powder preparation

The composition of the material was $BaZr_{0.1}Ce_{0.7}Y_{0.1}Yb_{0.1}O_{3-\delta}$. For convenience, in this study, the powder prepared by the conventional solid state reaction method was abbreviated as BZCYYb-SSR, and the EDTA-assisted GNP one as BZCYYb-GNP, respectively. The preparation procedure of BZCYYb-GNP is illustrated in Fig. 1. Firstly, 0.01 mol of ethylene diamine tetraacetic acid (EDTA) was mixed with 60 ml of 1 N NH_4OH solution to make EDTA-NH_3 buffer solution. Then, 0.1 mol $Ba(NO_3)_2$ and 0.01 mol $Zr(NO_3)_4 \cdot 5H_2O$ were added to the buffer solution under heating and stirring until forming a light yellow mixed solution. At the same time, 0.05 mol Y_2O_3 and 0.05 mol Yb_2O_3 were dissolved in nitric acid to form a mixed solution under heating and strong stirring and 0.07 mol $Ce(NO_3)_3 \cdot 6H_2O$ was added subsequently. Then the above two mixed solutions were mixed together after stirring for certain time followed by introducing 0.32 mol glycine (all above chemical reagents are of high purity). The pH value of the solution was adjusted to 6–7 by adding further amounts of 1 N NH_4OH solution. The mole ratio of total metal ions:glycine:EDTA was controlled to be around 2:3.2:1. Precipitation might occur after glycine addition, NH_4OH solution was then added to adjust the pH value to 6–7, and the solution became transparent immediately. EDTA–NH_3 and glycine formed a buffering solution; therefore the pH value of the system successfully sustained around 6 during the whole process. With the evaporating of water, a yellow gel was obtained. After the gel was placed in an oven at 650 °C, the combustion reaction took place within a few seconds, forming the primary powders in light yellow, which were subsequently calcined at various temperatures, viz. 800, 900, 1000, 1100 and 1200 °C for 2 h to obtain the powders with final composition.

2.2. Characterisation

The fine powders sintered at 800 °C for 2 h were ball-milled by zirconia balls in ethanol medium overnight to break up any agglomerations which formed during the high temperature calcination process. The as-prepared powders were pressed into pellets in a stainless steel mold (15 mm in diameter) and rectangular bar samples for the followed thermal expansion behavior test under an isostatical pressure of 538 MPa. These green pellets and rectangu-

lar bar samples were sintered in a SiC muffle oven at 1280 and 1400 °C for 10 h, respectively. The densities of the sintered samples were determined by the Archimedes method.

The Brunauer–Emmett–Teller specific surface area (S_{BET}) of the as-prepared powders was determined through a five-point nitrogen adsorption isotherm at 77 K (ASAP2020, Micromeritics Instruments Corp.) after degassing the powder sample with nitrogen at 300 °C for 2 h. Assuming spherical, monodisperse primary particles with homogeneous density, the average particle size (D_{BET}) in microns is equal to $6/(S_{BET}) \times \rho$, where ρ is the density of the powders. The phase compositions of the as-synthesized powders were identified by X-ray diffraction (XRD) analysis on Rigaku D/max-2000 X-ray diffractometer with monochromatic Cu Kα radiation (45 kV, 50 mA). The microstructures including particle morphology, polished surfaces of the sintered samples were observed using a scanning electron microscope (SEM, HITACHI, S-4700) coupled with INCA energy-dispersive X-ray spectroscopy (EDX). The thermal expansion of the sintered samples and the linear shrinkage of the BZCYYb green rectangular bar in air were studied using a NETZSCH DIL 402PC dilatometer and the thermal expansion in Ar was tested by a NETZSCH DIL 402C at heating rate of 5 °C min^{-1}.

For conductivity measurement, Pt paste was coated on the BZCYYb-GNP pellet and sintered at 800 °C for 0.5 h to remove the organism, and then Pt electrode was prepared. Ag wire was attached to the Pt electrode. The ionic conductivities of BZCYYb-GNP in humidified oxygen, in humidified hydrogen and in air were investigated by AC impedance spectroscopy from 400 to 800 °C using a potentiostat/galvanostat (model PARSTAT® 2273, Princeton applied research). The impedance frequency range was 10 mHz to 10 MHz with a signal amplitude of 5 mV. The impedance fitting analysis was controlled with software Zsimpwin.

3. Results and discussion

3.1. X-ray diffraction and microstructure

The SEM micrograph of the BZCYYb-GNP powder calcined at 800 °C for 2 h is shown in Fig. 2. The particle of powder is highly porous and the pore size varied from tens of nano-meters to several microns. The fill density of the "foam" powder is estimated to be about 0.071 g cm^{-3}. The powder has the specific surface area of 9.59 m^2 g^{-1} and the average diameter of about 42 nm as determined by BET measurement, which indicates that this powder is capable of being sintered at lower temperature. Such low fill density makes it possible to fabricate dense BZCYYb electrolyte membrane through the simple drying pressure [24].

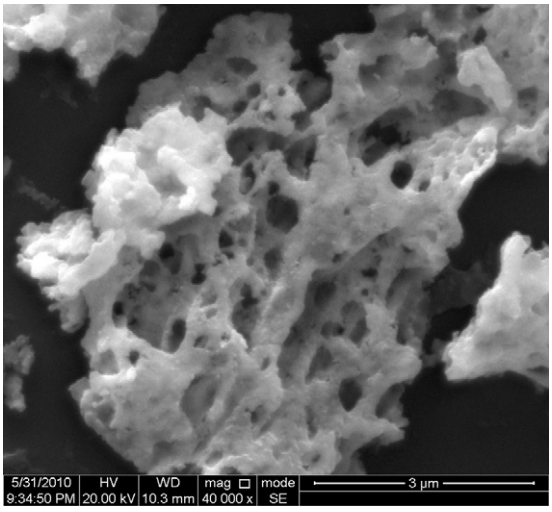

Fig. 2. SEM micrograph of a highly porous "foam" BZCYYb particle after calcined at 800 °C for 2 h.

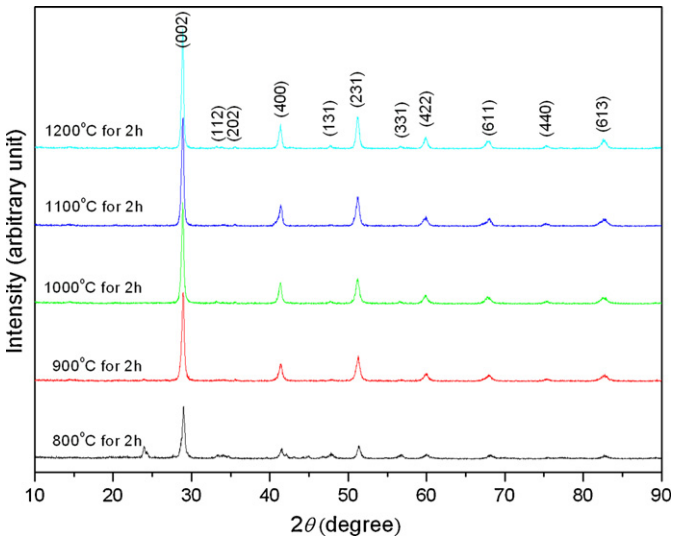

Fig. 3. XRD patterns of BZCYYb powders calcined at various temperatures ranging from 800 to 1200 °C.

The room temperature X-ray diffraction patterns of the BZCYYb-GNP powders calcined at various temperatures are shown in Fig. 3. Highly phase pure perovskite of BZCYYb prepared by the EDTA-assisted GNP was obtained when the calcination was carried out at 900 °C or above. No any secondary phase was detected in the calcined sample BZCYYb-GNP. The single-phase perovskite was obtained after being calcined at 900 °C for 2 h, and the sintering temperature was far lower than those prepared by solid-state reaction method as a result of the better distribution of all starting materials in mixture and the more feasible kinetic condition for the reaction [14,25]. The crystallinity increased with increasing calcining temperature. That low temperature at which the perovskite phase appeared is interesting and important, since this implies that one can synthesize the BZCYYb powders with weak agglomeration at low temperatures.

The linear shrinkage of the pressed green BZCYYb-GNP measured from 35 to 1510 °C in air and the derived curve of the linear shrinkage are shown in Fig. 4. The shrinkage during sintering will reflect the sintering ability of the as-calcined powders. From Fig. 4 it can be seen that an obvious increase of the linear shrinkage

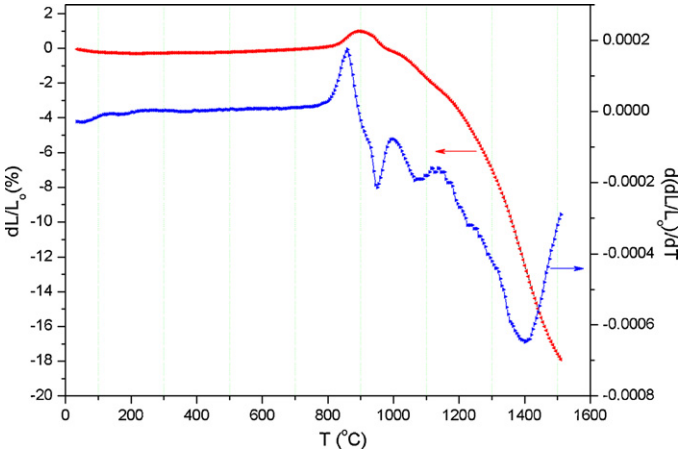

Fig. 4. Linear shrinkage of the pressed green BZCYYb-GNP measured from 35 to 1510 °C in air and the derived curve of the linear shrinkage.

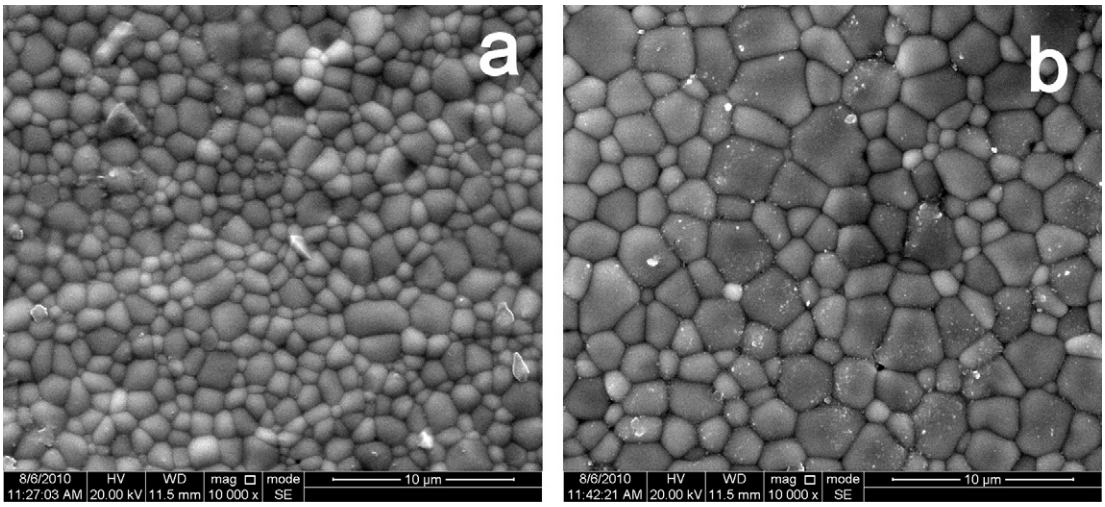

Fig. 5. SEM micrographs of the surfaces of the BZCYYb-GNP pellets after sintered at (a) 1280 °C and (b) 1400 °C for 10 h, respectively.

began from 900 °C. The total shrinkage reached 12.4% when the temperature was as high as 1400 °C. There was an interesting phenomenon of linear expansion occurred when the temperature was approached to 820 °C. As shown in the XRD patterns above, the resultant BZCYYb-GNP powders were not crystallized when calcined at 800 °C. The process of crystallization was occurred between 800 and 900 °C, which probably resulted in the volume change of about 1%. The derived curve of the linear shrinkage is also plotted in showing the $d(dL/L_0)/dT$ curve of the compacted green BZCYYb-GNP pellet. There are four shrinkage rate peaks in the curve, of which the corresponding temperatures for the four peaks are 860, 950, 1070 and 1400 °C, respectively. 860 °C corresponds to the crystallization of the amorphous products into the perovskite BZCYYb phase and 1400 °C corresponds to sintering densification temperature.

To assess the densification of samples, the relative densities of samples sintered at 1280 and 1400 °C for 10 h were measured. For each experiment, five parallel measurements were carried out; the average values were then obtained. In this experiment, the absolute value of the error was strictly less than 6‰. In Fig. 5, the SEM micrographs of the pellets for the selected sintering conditions show that dense materials can be obtained after sintering in air, suggesting that the present powders had higher sintering ability, especially when compared with the commonly used conventional solid state reaction. Lower sintering temperature may extraordinarily reduce the cost of fabrication. Most of all, lower sintering temperature will make it feasible to co-sinter anode/electrolyte/cathode three-layer structure of SOFCs and minimize the interfacial resistance which as one of the major challenges in co-firing usually makes large contribution to the total cell resistance at reduced temperatures [26]. It is seen from Fig. 5a that the BZCYYb-GNP sintered at 1280 °C for 10 h appears to be dense except for a few pinholes. The porosity is still visible on surface of the sample. The pores with around 0.3 μm are observed. The corresponding relative density reached as high as 96.8%. When the sample BZCYYb-GNP was sintered at 1400 °C for 10 h, almost no remaining pore was observed on the surface of the sample, and the higher relative density of 98.4% was achieved as shown in Fig. 5b. These results indicate that EDTA-assisted GNP method has produced a high quality BZCYYb electrolyte material at low sintering temperature.

3.2. Electrical properties

In SOFCs, the electrolyte material is exposed to both oxidizing and reducing atmospheres. Consequently, the ionic conductivity under both conditions was investigated after the dense BZCYYb-GNP was obtained through sintering at 1400 °C for 10 h as confirmed by the above relative density and SEM images. Fig. 6 shows Arrhenius plots of ionic conductivity for BZCYYb-GNP sample which were tested under different circumstances. The values of the conductivity for the sample under various sintering conditions are shown in Table 1. In air and humidified oxygen, the activation energies for the ionic conductivity are 66.1 and 68.9 kJ mol^{-1}, respectively. However, it could be seen from Fig. 6c that there were different activation energies for ionic conductivity in the high and low temperature ranges under the humidified hydrogen condition. A similar result has been reported by Peng et al. on the ionic conductivity of bulk material $BaCe_{0.8}Sm_{0.2}O_{2.90}$ [27]. The activation energy in high temperature range for sample BZCYYb sintered at 1400 °C for 10 h were 41.7 kJ mol^{-1}, and the low temperature range one was 75.7 kJ mol^{-1}. The plot had two regimes with different slope intersecting at about 600 °C. As a mixed conductor, BZCYYb shows not only proton but also oxide-ion conduction under the fuel cell operating conditions. The protonic conductivity was reported to preponderate over oxide-ion conductivity at temperature lower than 800 °C and to be about one order of magnitude higher than that at temperature lower than 600 °C. The dominance of protonic conductivity at operating temperature might suggest that the intersection of conductivity origins not from the change of conducting species but from the dependence of proton defects concentration

Table 1
Ionic conductivities and activation energies of the sample BZCYYb-GNP under various testing conditions.

	Ionic conductivity (S cm^{-1})				Activation energy (Ea, kJ mol^{-1})
	800 °C	700 °C	600 °C	500 °C	
In humidified hydrogen	0.113	0.075	0.047	0.014	75.7 (400–600 °C) 41.7 (600–800 °C)
In air	0.148	0.086	0.040	0.013	66.1
In humidified oxygen	0.207	0.101	0.045	0.015	68.9

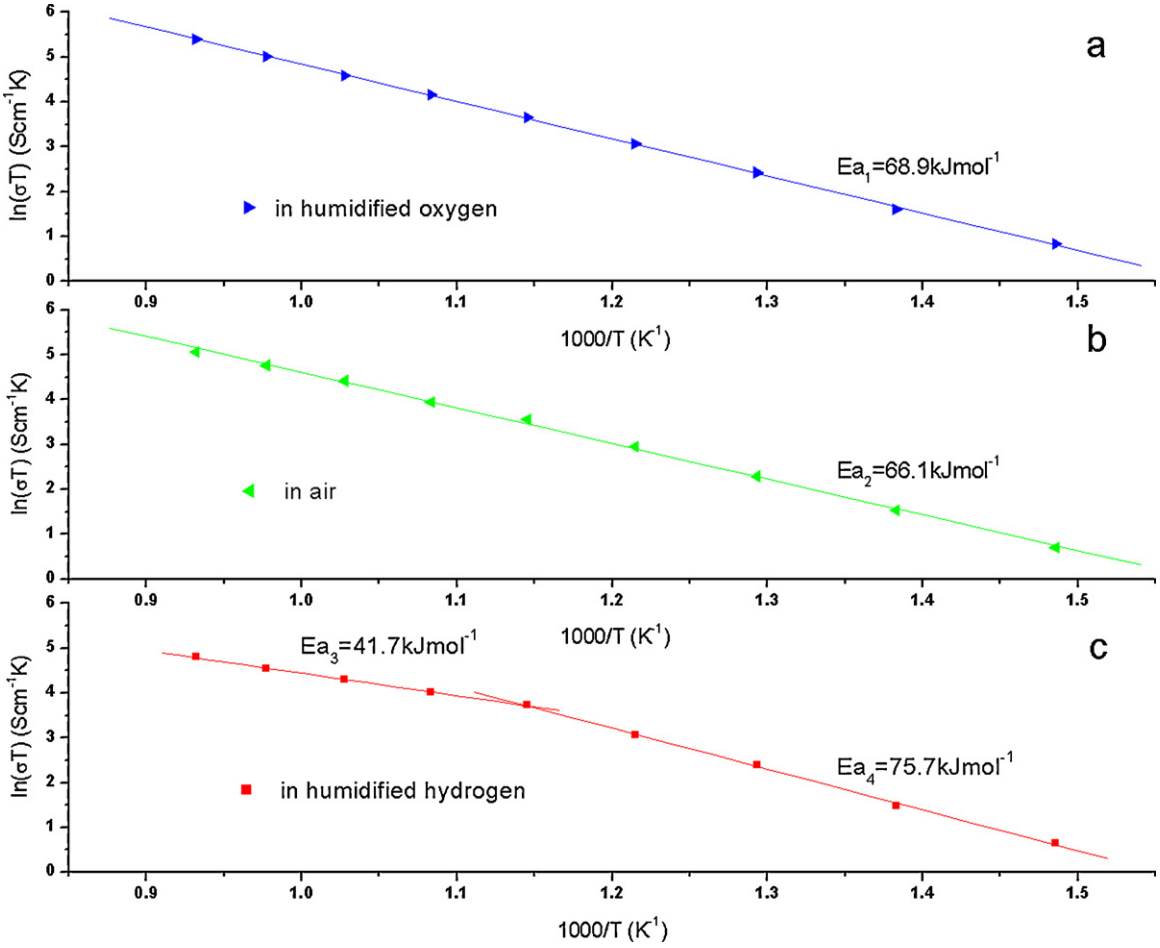

Fig. 6. Arrhenius plots of BZCYYb-GNP conductivities under different circumstances determined by impedance spectra at 400–800 °C (a) in humidified oxygen (with ~3 vol% H_2O), (b) in air, (c) in humidified hydrogen (with ~3 vol% H_2O). *Ea* is the activation energy of conductivity.

on temperature, which is entirely consistent with literature [10]. Amsif et al. [28] contributed the enhancement of the conductivity in humidified hydrogen to the presence of proton contribution at low temperature. As the temperature is elevated the material dehydrates, reducing the protonic contribution and accordingly the conductivity is less dependent on the atmosphere at high temperature. On the other hand, when used as the electrolyte in a SOFC, the electronic conductivity of BZCYYb is relatively small, and even smaller so at lower temperatures [14]. When used as a component for the anode and exposed to hydrogen and water, however, both the ionic defects ($OH_O^{\bullet}$ and $V_O^{\bullet\bullet}$) and the electronic defects (e'

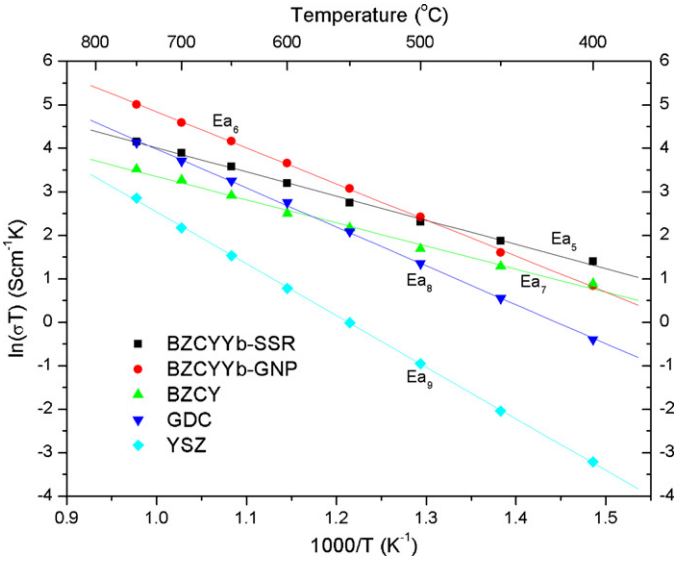

Fig. 7. Arrhenius plots of BZCYYb-GNP conductivities as measured at 400–750 °C in humidified oxygen (with ~3 vol% H_2O). The conductivities of electrolyte materials BZCYYb-SSR, BZCY, GDC, and YSZ are adapted from Ref. [14].

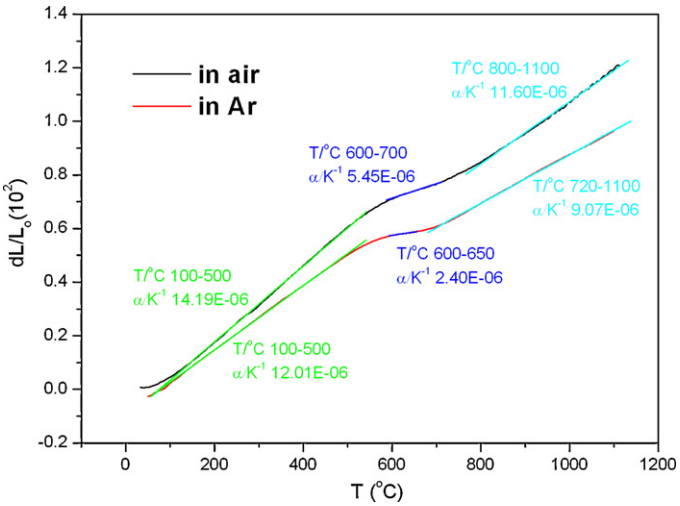

Fig. 8. Thermal expansion curves of sample BZCYYb-GNP in the temperature range of 30–1100 °C measured in various circumstances.

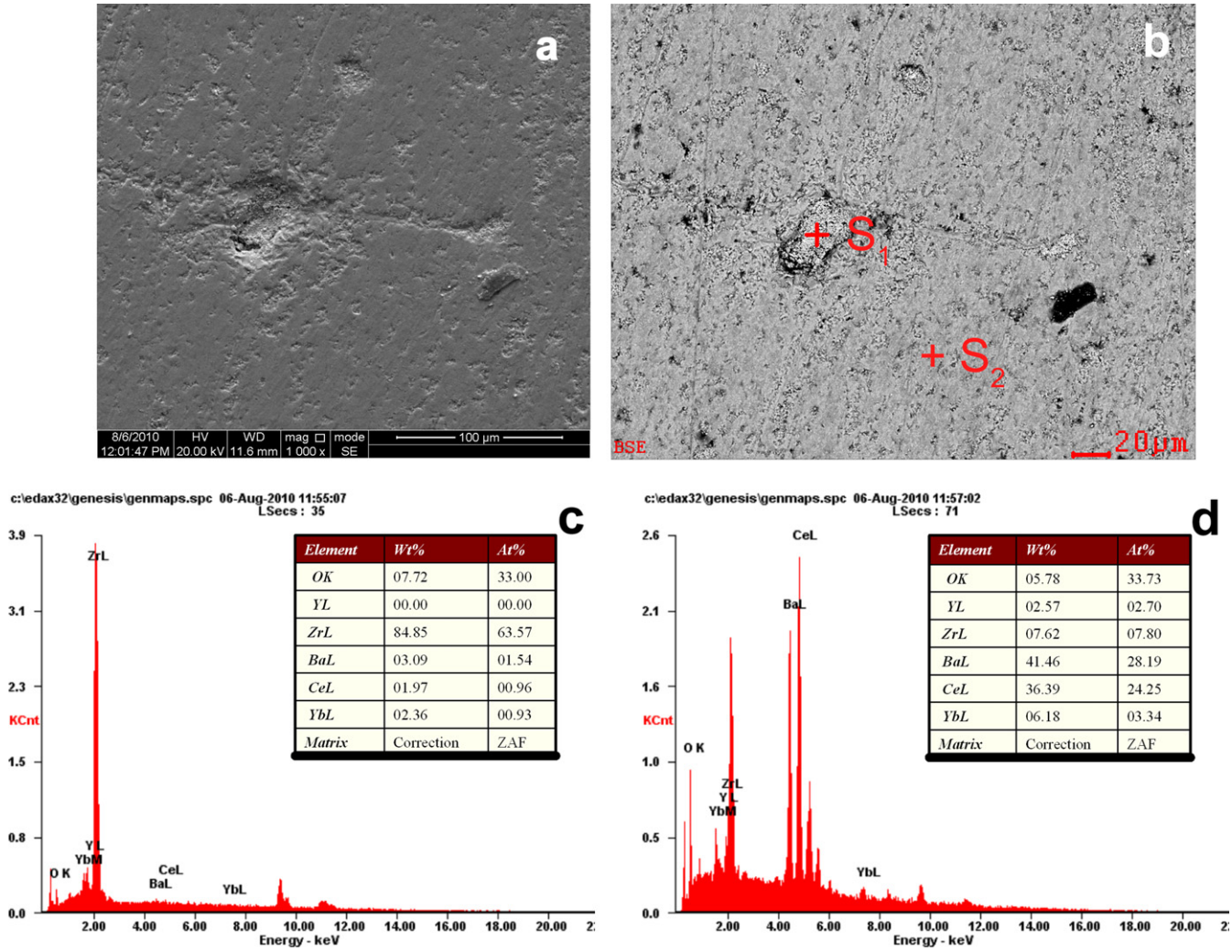

Fig. 9. (a) An SEM image of the polished surface of BZCYYb-GNP pallet after sintering at 1400 °C for 10 h. (b) The SEM micrograph (backscattered mode) of BZCYYb-GNP obtained from (a). (c) and (d) EDX spectra of two different spots S1 and S2 obtained from the polished surface of BZCYYb-GNP.

and $h^{\bullet}$) may coexist, enhancing the electrical conductivity especially in higher temperatures. As shown in Table 1, conductivities of BZCYYb under humidified hydrogen circumstances were obtained as 0.014, 0.047, 0.075 and 0.113 S cm^{-1} at 500, 600, 700 and 800 °C, respectively. The ionic conductivities in humidified oxygen were 0.015, 0.045, 0.101 and 0.207 S cm^{-1} at 500, 600, 700 and 800 °C, respectively. The conductivities both in humidified oxygen and in humidified hydrogen were much higher than those by the conventional solid state reaction, which was contributed to the higher sintering ability of the as-prepared ultrafine powders [14].

Fig. 7 shows the Arrhenius plots of BZCYYb-GNP conductivities as measured from 400 to 750 °C in humidified oxygen (with ~3 vol% H_2O). For comparison, the Arrhenius plots of ionic conductivities for electrolyte materials BZCYYb-SSR, BZCY, GDC, and YSZ were also plotted in this figure. Table 2 specifies the activation energies of BZCYYb-GNP, BZCYYb-SSR, BZCY ($BaZr_{0.1}Ce_{0.7}Y_{0.2}O_{3-\delta}$), GDC ($Gd_{0.1}Ce_{0.9}O_{2-\delta}$), and YSZ ($Y_{0.15}Zr_{0.85}O_{2-\delta}$). It can be seen that as a promising candidate for electrolyte in low-temperature SOFCs the proton conductor BZCY had the smallest activation energy, however, the activation energy for the conventional oxygen ion conductor YSZ appeared to the biggest one of 98.8 kJ mol^{-1}. The difference between activation energies maybe resulted from the different species of current carriers in YSZ and BZCY. The activation energies for BZCYYb samples prepared by solid state reaction and EDTA-assisted GNP were 46.2 and 68.9 kJ mol^{-1}, respectively, which probably derived from the different grain sizes and different grain boundaries.

3.3. Thermal expansion behavior

Electrolyte materials must have a compatible coefficient of thermal expansion (CTE) with the other cell components to minimize thermal stresses because SOFCs are running at high temperatures. As far as the barium cerate-based materials is concerned, there are few reports about CTE. Fig. 8 shows the thermal expansion behaviors of the samples BZCYYb-GNP from 30 to 1100 °C in air and in Ar. The samples BZCYYb-GNP were sintered at 1400 °C for 10 h. It could be seen that some inflections were observed at the curves both in air and in Ar. This indicates that there probably were structure transformations or phase changes occurred in this temperature range. The inflections occurred between 500 and 800 °C, indicating that the structure transformations or phase changes took place in this temperature range. As shown in Fig. 8, when measured in air, the CTEs for the BZCYYb-GNP were 14.19×10^{-6} K^{-1}, 5.45×10^{-6} K^{-1} and 11.60×10^{-6} K^{-1} in temperature range of 100–500 °C, 600–700 °C and 800–1100 °C, respectively. Similar behaviors occurred to that tested in Ar. The CTEs were 12.01×10^{-6} K^{-1}, 2.40×10^{-6} K^{-1} and 9.07×10^{-6} K^{-1} in temperature ranges of 100–500 °C, 600–650 °C and 720–1100 °C, respectively.

Table 2
Activation energies of BZCYYb-GNP, BZCYYb-SSR, BZCY, GDC, and YSZ as measured at 400–750 °C in humidified oxygen (with ~3 vol% H_2O).

Electrolyte	BZCYYb-GNP	BZCYYb-SSR	BZCY	GDC	YSZ
Activation energy (kJ mol^{-1})	68.9	46.2	44.3	74.4	98.8

3.4. Energy dispersive spectrum analysis

Patnaik and Virkar [29] reported zirconia aggregated in the bulk materials when they investigated the effect of doping potassium on the A-site of $BaZrO_3$ for application as a high-temperature proton conductor. The formation of cracks around the precipitated monoclinic zirconia grains occurred due to the tetragonal to monoclinic transformation of zirconia during cooling. The SEM images of the sintered sample showed that the amount of second phase (tetragonal zirconia) was only ~4 vol%. The authors assumed that such a small amount of the secondary phase had minimal effect on the electrical properties of the materials. To check the chemical composition of the sintered sample, the energy dispersive spectrum (EDX) analysis was performed for various micro-area surfaces of the sample as shown in Fig. 9b. The results of the EDX analysis for two different spots S_1 and S_2 obtained from the polished surface of BZCYYb-GNP are shown in Fig. 9c and d. As could be seen, there were the zirconia aggregations in the bulk material as the EDX results illustrated from various micro-area surface after the BZCYYb-GNP pellet was sintered at 1400 °C for 10 h. XRD of the sample BZCYYb-GNP sintered at 1400 °C for 10 h was performed in order to confirm the existence of zirconia, however, the results indicated that no peaks of zirconia were found. This was contributed to the small amount of zirconia below the detecting limit of X-ray diffractometer. The disagreement between the experimental and the nominal stoichiometric indexes indicates the structural stability and the homogeneity of composites are likely to be the dominating impacts on the electrical property and thermal expansion behavior as discussed above. In the next step, we will focus on the investigation of structural phase transition behaviors and stability of BZCYYb by thermal analyses and high-temperature X-ray diffraction and the results will be published in another paper.

4. Summary and conclusions

Recently, barium cerate-based electrolyte materials have attracted much attentions and shown great advantages over the conventional zirconia-based electrolyte materials. In this paper, the novel mixed ion conductor BZCYYb was prepared through the EDTA-assisted GNP in order to obtain ultrafine ceramic powders with high sintering ability. The single-phase perovskite was obtained after calcining the as-prepared powders at 900 °C for 2 h. The significantly lower sintering temperature than that by solid-state reaction method resulted from the better distribution of the starting materials and the more feasible kinetic conditions for the reaction. The relative densities 96.8% and 98.4% of the pressed pellets were reached after sintered at 1280 and 1400 ° for 10 h, respectively. The activation energies for the ionic conductivity in air and humidified oxygen were 66.1 and 68.9 kJ mol^{-1}, respectively. However, there were different activation energies in the testing temperature range in humidified hydrogen. The ionic conductivities in humidified hydrogen and in humidified oxygen at 800 °C were 0.113 and 0.207 S cm^{-1}, respectively. The thermal expansion curves showed inflections between 500 and 800 °C, reflecting structural transformations or phase changes were probably occurred in this temperature range. The zirconia aggregation in the bulk material was verified by the SEM backscattered micrographs and EDX spectra, which is possibly responsible for the higher activation energies and peculiar thermal expansion behavior. Results indicated the investigation on structural phase transition behavior and stability should be concentrated on afterwards.

Acknowledgements

This project is financially supported by Project (HIT.NSRIF.2009085) Supported by Natural Scientific Research Innovation Foundation in Harbin Institute of Technology, Development Program for Outstanding Young Teachers in Harbin Institute of Technology (No. HITQNJS.2008.056), China Postdoctoral Science Foundation (No. 20070420865), and Natural Science Foundations of China (No. 90510006 and 50821002).

References

[1] A.J. Jacobson, Chem. Mater. 22 (2010) 660.
[2] T.P. Chen, J.D. Wright, K. Krist, in: U. Stimming, S.C. Singhal, H. Tagawa, W. Lehnert (Eds.), SOFC V, The Electrochemical Society, Pennington, NJ, 1997, p. 69, PV 97-40.
[3] O. Yamamoto, Electrochim. Acta 45 (2000) 2423.
[4] H.L. Tuller, in: H. Tuller, J. Schoonman, I. Riess (Eds.), Oxygen Ion and Mixed Conductors and their Technological Applications, Kluwer (NATO ASI series), Dordrecht, 2000, p. 245.
[5] P. Holtappels, F.W. Poulsen, M. Mogensen, Solid State Ionics 135 (2000) 675.
[6] B.C.H. Steele, J. Mater. Sci. 36 (2001) 1053.
[7] D.J.L. Brett, A. Atkinson, N.P. Brandon, S.J. Skinner, Chem. Soc. Rev. 37 (2008) 1568.
[8] A. Sammells, R. Cook, J. White, J. Osborne, R. MacDuff, Solid State Ionics 52 (1992) 111.
[9] A.K. Demin, P.E. Tsiakaras, V.A. Sobyanin, S.Yu. Hramova, Solid State Ionics 555 (2002) 152.
[10] K.D. Kreuer, Annu. Rev. Mater. Res. 33 (2003) 333.
[11] D. Hirabayashi, A. Tomita, S. Teranishi, T. Hibino, M. Sano, Solid State Ionics 176 (2005) 881.
[12] C.D. Zou, S.W. Zha, M.L. Liu, M. Hatano, M. Uchiyama, Adv. Mater. 18 (2006) 3318.
[13] H. Iwahara, T. Yajima, H. Uchida, K. Morimoto, Proc. 2nd Intern. Symp., SOFC, Athens, Greece, 1991, pp. 229–235.
[14] L. Yang, S.Z. Wang, K. Blinn, M.F. Liu, Z. Liu, Z. Cheng, M.L. Liu, Science 326 (2009) 126.
[15] S.V. Chavan, P.U. Sastry, A.K. Tyagi, Scripta Mater. 55 (2006) 569.
[16] N. Kasapoglu, A. Baykal, Y. Koseoglu, M.S. Toprak, Scripta Mater. 57 (2007) 441.
[17] Y. Chen, W. Zhou, Z. Shao, N. Xu, Catal. Commun. 9 (2008) 1418.
[18] T. Tabakova, V. Idakiev, J. Papavasiliou, G. Avgouropoulos, T. Ioannides, Catal. Commun. 8 (2007) 101.
[19] D. Hari Prasad, J.W. Son, B.K. Kim, H.W. Lee, J.H. Lee, J. Eur. Ceram. Soc. 28 (2008) 3107.
[20] L.A. Chick, L.R. Pedersen, G.D. Maupin, J.L. Bates, L.E. Thomas, G.J. Exarhos, Mater. Lett. 10 (1990) 6.
[21] N.J. Hess, G.D. Maupin, L.A. Chick, D.S. Sunberg, D.E. Mccreedy, T.R. Armstrong, J. Mater. Sci. 29 (1994) 1873.
[22] M.W. Murphy, T.R. Armstrong, P.A. Smith, J. Am. Ceram. Soc. 80 (1997) 165.
[23] L.R. Pederson, G.D. Maupin, W.J. Weber, D.J. McReady, R.W. Stephens, Mater. Lett. 10 (1991) 437.
[24] L. Yang, C.D. Zuo, M.L. Liu, J. Power Sources 195 (2010) 1845.
[25] J.F. Xue, Y. Shen, Q.J. Zhou, T.M. He, Y.H. Han, Int. J. Hydrogen Energy 35 (2010) 294.
[26] C.R. Xia, M.L. Liu, Solid State Ionics 152 (2002) 423.
[27] R.R. Peng, Y. Wu, L.Z. Yang, Z.Q. Mao, Solid State Ionics 177 (2006) 389.
[28] M. Amsif, D. Marrero-Lopez, A. Magraso, J. Pena-Martinez, J.C. Ruiz-Morales, J. Eur. Ceram. Soc. 29 (2009) 131.
[29] A.S. Patnaik, A.V. Virkar, J. Electrochem. Soc. 153 (7) (2006) A1397.